Tu 11 03

Non-linear Least-squares Reverse-time Migration

G. Yao* (Imperial College London) & H. Jakubowicz (Imperial College London)

SUMMARY

Migration attempts to produce an image of the subsurface by reversing the propagation effects in seismic data. Although in principle this requires the inverse of a modelling operator, in practice the adjoint of the modelling operator is used instead. This applies to nearly all migration methods, including reverse-time migration. In cases where the data are subject to significant aliasing, truncation, or noise, the adjoint of a modelling operator is not a good approximation to the inverse, and this degrades the resolution of the final migrated image.

At last year's meeting we presented a matrix formulation of least-squares reverse-time migration which provides an improved approximation to the inverse of the modelling operator, and which in turn results in more accurate amplitudes and higher resolution. Unfortunately, the matrix formulation, while very efficient in 2D, is currently computationally impractical for 3D data. In this paper, we present a non-linear least-squares reverse-time migration algorithm which generates the predicted data directly from the reflectivity without assuming they are linearly related. This algorithm retains the benefits of our previous approach, but is also feasible in 3D. In addition, the new formulation opens up the possibility of generating improved velocity estimates as part of the migration process.

Introduction

Migration attempts to produce an image of the subsurface by reversing the propagation effects in seismic data. Although in principle this requires the inverse of a modelling operator, in practice the adjoint of the modelling operator is used instead. This applies to nearly all migration methods, including reverse-time migration (RTM). In general, the adjoint of a modelling operator is not a good approximation to the inverse operator (Claerbout, 1992), and this degrades the quality and resolution of the final migrated image.

An improved approximation to the inverse operator can be obtained using a least-squares approach (Nemeth *et al*., 1999; Kühl and Sacchi, 2001; Kaplan *et al*., 2010; Dai and Schuster, 2010). Yao and Jakubowicz (2012) recently developed a matrix-based implementation of least-squares reverse-time migration (MLSRTM) which combines the advantages and accuracy of RTM with the improved amplitude treatment inherent in least-squares imaging. However, while MLSRTM is very efficient in 2D, it requires a large amount of memory, and is impractical for 3D data. In this paper we present an alternative formulation of least-squares reverse-time migration which generates the predicted data directly from the reflectivity without assuming a linear relationship, and which is practical in 3D. We refer to this method as non-linear least-squares reverse-time migration (NLLSRTM).

Theory

In seismic exploration, the reflection data can be expressed as

$$D(\boldsymbol{x_r}, \omega) = \int G(\boldsymbol{x_r}|\boldsymbol{x}; \omega) R(\boldsymbol{x}) G(\boldsymbol{x}|\boldsymbol{x_s}; \omega) S(\omega) d\boldsymbol{x}\,, \tag{1}$$

where $G(\boldsymbol{x}|\boldsymbol{x_s}; \omega)$ and $G(\boldsymbol{x_r}|\boldsymbol{x}; \omega)$ are the source and receiver Green's function respectively, $R(\boldsymbol{x})$ is the true reflectivity, $S(\omega)$ is the source wavelet and $D(\boldsymbol{x_r}, \omega)$ is the recorded data.

The reflectivity $R(\boldsymbol{x})$ can be extracted from the recorded data by optimising the objective function $\varphi_D(I(\boldsymbol{x}))$, where

$$\varphi_D(I(\boldsymbol{x})) = \frac{1}{2} \| < D(\boldsymbol{x_r}) > - D(\boldsymbol{x_r}) \|^2, \tag{2}$$

and $< D(\boldsymbol{x_r}) >$ and $D(\boldsymbol{x_r})$ are respectively the predicted and recorded data, and $I(\boldsymbol{x})$ is the inverted reflectivity (i.e. the migrated image). Converting Equation 2 into a matrix form, the gradient of the objective function with respect to I is then given by

$$\frac{\partial \varphi_D(I(\boldsymbol{x}))}{\partial I(\boldsymbol{x})} = Re\{[GS]^{\dagger}[G^{\dagger}(GI(\boldsymbol{x})GS - D(\boldsymbol{x_r}))]\}, \tag{3}$$

where "Re" indicates the real part of a complex number.

Given the gradient of the objective function, the reflectivity model can be iteratively updated as

$$I_{n+1}(\boldsymbol{x}) = I_n(\boldsymbol{x}) + \alpha \boldsymbol{q}, \tag{4}$$

where α is an optimum step length, and $\boldsymbol{q}$ is the update direction.

Implementation

Our implementation of NLLSRTM incorporates three main features. The first is suppression of high-wavenumber artefacts using a roughness constraint (Bube and Langham, 2008), while the second is an option to weight later arrivals; this latter feature enhances deeper reflectors, ensures that the calculations are not dominated by strong energy at early times in the data, and also helps improve the speed of convergence. Finally, we use the nonmonotonic Barzilai-Borwein gradient solution technique (Barzilai and Borwein, 1988; Wang and Yang, 2010); although this converges slightly more slowly than either the non-linear conjugate-gradient or quasi-Newton methods, it requires significantly fewer calculations at each step, and also converges much faster than the non-linear steepest-descent method. The entire implementation requires a similar amount of memory to conventional RTM, and, in contrast to MLSRTM, is therefore suitable for application in 3D.

Examples

We will demonstrate our implementation of NLLSRTM using a model consisting of nine point diffractors embedded in a medium with a constant velocity of 2000 m/s (Figure 1a); a similar model is also used in Yao and Jakubowicz (2012). Figure 1d shows a shot record simulated over the model for a surface source at x=500 m, and receivers every 10 m along the surface; the source signature is a 30 Hz Ricker wavelet, and the direct arrivals, which do not contribute to the imaging, have been removed. Figures 1b and 1c show the results of applying conventional RTM and NLLSRTM to the data in Figure 1d, together with additional shots at x=200 m and x=800 m, while Figures 1e and 1f show the modelled shot data corresponding to Figure 1d for the RTM and NLLSRTM images.

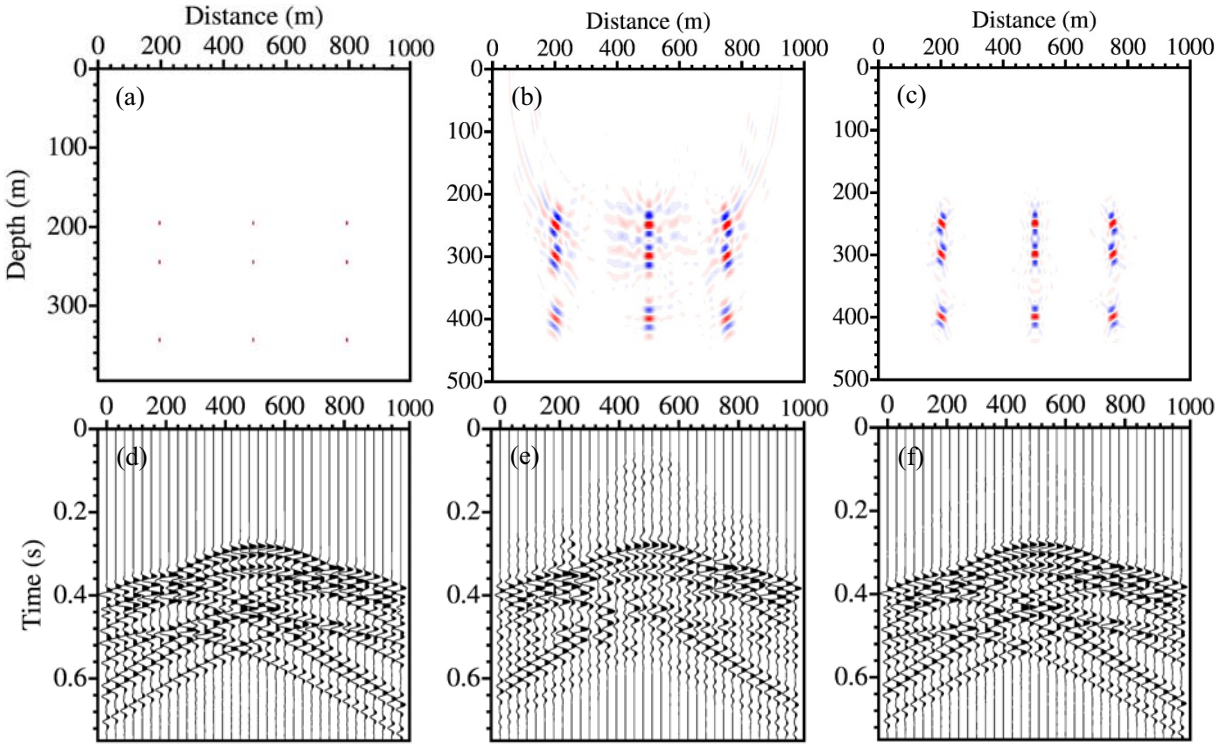

Figure 1 *(a) Model containing nine point diffractors embedded in a medium with a constant velocity of 2000 m/s; (b) RTM for three shot records from the model shown in (a), and (c) the same as (b) but for NLLSRTM. (d) A shot record for a source at x=500 m; (e) the equivalent implied shot record for RTM, and (f) NLLSRTM. All the horizontal axes are distances in meters.*

Figure 1 shows that NLLSRTM has two immediate advantages relative to RTM. First, the diffractors in the NLLSRTM image are better resolved, and have fewer sidelobes, than those from RTM. This is because the imaging condition for RTM is based on crosscorrelation, and therefore retains (actually amplifies) the imprint of the source signature. By contrast, in matching the image and recorded data, NLLSRTM compensates for the source signature, and is equivalent to using a deconvolution imaging condition (Yao and Jakubowicz, 2012). Second, the amplitudes of the later arrivals in the modelled NLLSRTM data are closer to those in the recorded data than in the case of RTM. This is because RTM uses adjoint, rather than inverse, operators, and these fail to correct adequately for geometrical spreading. More generally, these characteristics are intrinsic to the combination of least-squares imaging and reverse-time migration, and can be obtained with other implementations, including MLSRTM (Yao and Jakubowicz, 2012).

Practical Benefits

In addition to providing higher resolution and more accurate amplitudes, NLLSRTM also has other advantages over conventional migration. In particular, whereas conventional migration generates artefacts when the input data are spatially aliased, NLLSRTM suppresses aliasing artefacts, and can therefore be used on relatively coarsely sampled data.

Figure 2a shows the FK spectrum of the shot record in Figure 1d, but with a trace spacing of 40 m (every fourth trace). In this case, the coarser sampling introduces wraparound and spatial aliasing, which in turn introduce artefacts when the data with the coarser trace spacing is migrated using conventional RTM (Figure 2b). By contrast, because the artefacts are inconsistent with implied model for Equation 2, the equivalent result from NLLSRTM (Figure 2c) appears unaffected by the spatial aliasing. Indeed, although not shown here, for models containing continuous reflectors, this feature of NLLSRTM can be further enhanced using the roughness constraint.

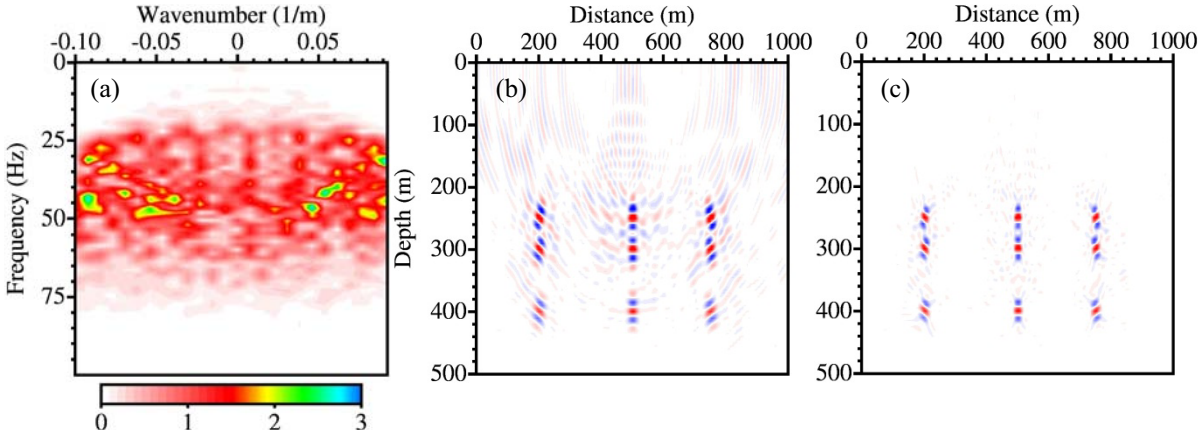

Figure 2 *(a) FK spectrum of the shot record in Figure 1d but with a trace spacing of 40 m. (b) Result of conventional RTM and (c) NLLSRTM for all three shots with a trace spacing of 40 m.*

A second important benefit of NLLSRTM is that it can help attenuate random noise. In particular, whereas conventional migration, including RTM, is a linear process, the objective function given by Equation 2 is nonlinear. Thus, whereas conventional imaging provides noise attenuation via the statistics of stacking data either before or after imaging, NLLSRTM has the potential for additional noise suppression. Figures 3b and c show the RTM and NLLSRTM images for the same three shots as used in Figure 1, but after Gaussian noise has been added with a signal-to-noise ratio of 2 (Figure 3a). Although both images are noisier than their noise-free counterparts (Figures 1b and 1c), the NLLSRTM result is much quieter than that for RTM. Furthermore, this applies despite the relatively small amount of data used in the migration.

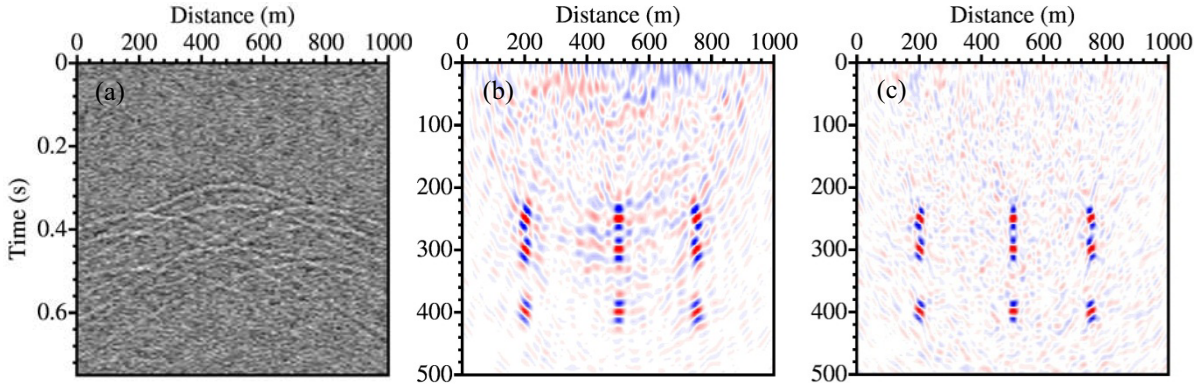

Figure 3 *(a) The same shot record as in Figure 1d, but with Gaussian random noise and a signal-to-noise ratio of 2. (b) Result of conventional RTM and (c) NLLSRTM for all three shot records. Compare Figures 3b and 3c with Figures 1b and 1c.*

Future Directions

While the above benefits of NLLSRTM are already substantial, it is possible that the method may also provide opportunities for other applications, including migration velocity estimation. Figure 4 shows how this might be done. Figures 4a and b show the results of NLLSRTM for the same data as in Figure 1, but with velocity errors of -5% (Figure 4a) and +5% (Figure 4b). As expected, using

incorrect velocities blurs the image, and is also introduces undermigration or overmigration. However, a plot of the residual errors from Equation 2 as a function of the percentage velocity error (Figure 4c) shows that velocity errors produce larger residuals, and that these are a minimum at the correct migration velocity. Moreover, Equation 3 shares a similar form to the gradient used in full waveform inversion (Virieux and Operto, 2009). As a result, it may be possible to use NLLSRTM not only to produce an improved image, but also to update and increase the accuracy of the migration velocities.

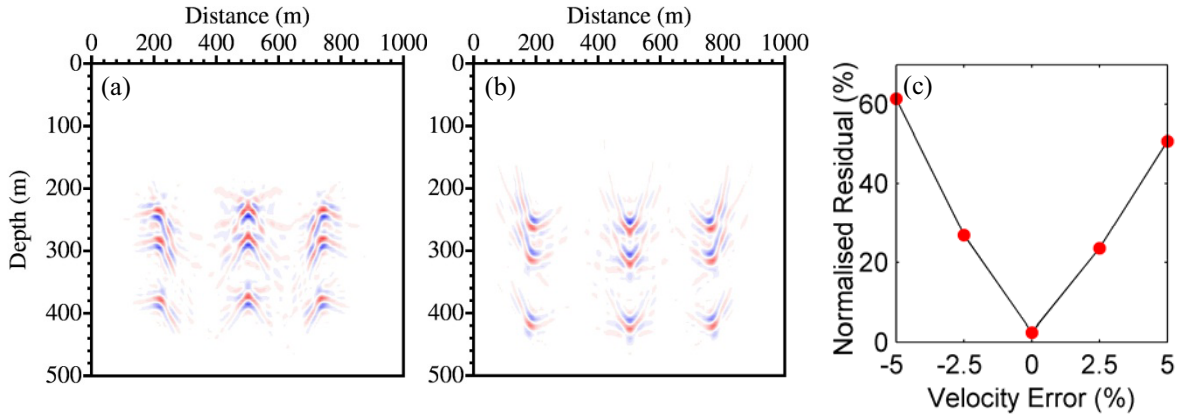

Figure 4 *NLLSRTM images of the same data as in Figure 1, but with (a) 95% and (b) 105% of the correct migration velocity. (c) Plot of the normalised residual against velocity error.*

Conclusions

We have shown that NLLSRTM has several benefits relative to conventional RTM. The least-squares formulation incorporates a deconvolution imaging condition which results in higher resolution and more accurate amplitudes, and can also help overcome spatial aliasing and suppress noise. The implementation described here is robust and stable, suitable for application in 3D, and may lead to methods of generating improved estimates of migration velocities.

Acknowledgements

The authors thank Professor Yanfei Wang and Dr Jingjie Cao for helpful discussions.

References

Barzilai, J. and Borwein, J.M. [1988] Two-Point Step Size Gradient Methods. *IMA journal of numerical analysis*, **8**, 141-148.

Bube, K.P. and Langan, R.T. [2008] A Continuation Approach to Regularization of Ill-Posed Problems with Application to Crosswell-Traveltime Tomography. *Geophysics*, **73**, VE337-VE351.

Claerbout, J. F. [1992] Earth Soundings Analysis: Processing Versus Inversion. *Blackwell Science*.

Dai, W. and Schuster, G.T. [2010] Multi-Source Wave-Equation Least-Squares Migration with a Deblurring Filter. *72nd EAGE Conference & Exhibition*, Expanded Abstracts, P276.

Kaplan, S.T., Routh, P.S. and Sacchi, M.D. [2010] Derivation of Forward and Adjoint Operators for Least-Squares Shot-Profile Split-Step Migration. *Geophysics*, **75** , S225-S235.

Kühl, H. and Sacchi, M.D. [2001] Generalized Least-Squares DSR Migration Using a Common Angle Imaging Condition. *71th Annual International Meeting, SEG*, Expanded Abstracts, 1025-1028.

Nemeth, T., Wu, C. and Schuster, G.T. [1999] Least-Squares Migration of Incomplete Reflection Data. *Geophysics*, **64**, 208-221.

Virieux, J. and Operto, S. [2009] An Overview of Full-Waveform Inversion in Exploration Geophysics. *Geophysics,* **74**, WCC1-WCC26.

Wang, Y. and Yang, C. [2010] Accelerating Migration Deconvolution Using a Nonmonotone Gradient Method. *Geophysics*, **75**, S131-S37.

Yao, G. and Jakubowicz, H. [2012] Least-Squares Reverse-Time Migration. *74nd EAGE Conference & Exhibition*, Expanded Abstracts, X043.